Nuclear Instruments and Methods in Physics Research A 657 (2011) 107–113

Contents lists available at ScienceDirect

Nuclear Instruments and Methods in Physics Research A

journal homepage: www.elsevier.com/locate/nima

Design and applications of an X-band hybrid photoinjector

J.B. Rosenzweig [a,*], A. Valloni [a,d], D. Alesini [b], G. Andonian [a,c], N. Bernard [a], L. Faillace [c], L. Ficcadenti [b], A. Fukusawa [a], B. Hidding [a], M. Migliorati [d], A. Mostacci [d], P. Musumeci [a], B. O'Shea [a], L. Palumbo [d], B. Spataro [b], A. Yakub [a]

[a] UCLA Dept. of Physics and Astronomy, 405 Hilgard Ave., Los Angeles, CA 90095, USA
[b] Istituto Nazionale di Fisica Nucleare, Laboratori Nazionali di Frascati, via Enrico Fermi 40, Frascati (RM), Italy
[c] RadiaBeam Technologies, LLC, 1717 Stewart Ave., Santa Monica, CA 90404, USA
[d] Dipartimento di Scienze di Base e Applicate per l'Ingegneria, Universita' degli Studi di Roma "La Sapienza", Via Antonio Scarpa 14, Roma (RM) 00185, Italy

ARTICLE INFO

Available online 23 June 2011

Keywords:
Photoinjector
Coherent radiation
Wakefield
Diffraction
Femtosecond

ABSTRACT

An INFN-LNF/UCLA/URLS collaboration is developing a hybrid photoinjector in X-band. This device is an integrated structure consisting of initial standing wave gun cells connected at the input coupler to a traveling wave section. This design nearly eliminates RF reflections from the SW section; further, a 90° phase shift in the accelerating field at the coupling cell gives strong velocity bunching. The current initiative in X-band follows an S-band hybrid, now proceeding to construction at LNF and high power testing/beam production measurements at UCLA. This S-band hybrid has 1.5 cell SW and 9 cell TW sections, and produces strongly compressed 3.5 MeV beam. It can be used for novel applications; here we discuss the production of an exponential energy spectrum extending from 1 to 12 MeV to simulate the effects of radiation belt environments on space-craft. It can be optionally used with a 3 m TW linac fed from RF output of the hybrid, to boost the energy to 22 MeV. While scaling the design from S-band to X-band is conceptually simple, practical limits require changes in both RF and magnetostatic designs. As the field is limited by RF breakdown to 200 MV/m peak field, the SW section must be expanded to 2.5 cells to reach 3.5 MeV; this permits flexibility in the solenoid design. We present beam dynamics simulations that show 6D phase space compensation at 7 pC: sub-0.1 mm mrad at the emittance minimum that occurs simultaneously with a longitudinal focus of <20 fs rms. We discuss applications ranging from multi-THz coherent radiation production to ultra-fast electron diffraction.

1. Introduction

It has long been recognized that in order to obtain high brightness electron beams from radio-frequency (RF) photoinjectors [1] – i.e. simultaneously possessing high charge, short pulse, and low emittance – the use of higher field amplitudes, particularly at the cathode, should be demanded [2]. The reasons for this are multi-fold and connected. First, in order to avoid pulse lengthening due to space-charge, one must launch a beam with low enough charge and sufficient transverse width so that the self-longitudinal electric field does not approach that of the applied RF electric field in amplitude [3,4]. This in turn causes the both thermal and collective contributions to the final transverse emittance to increase.

The currently employed 1.6 cell RF photoinjectors [5] are operated with peak on-axis fields just above 100 MV/m in S-band. While these electron sources have produced impressive results, enabling the development of the modern SASE FEL, as well as fundamental results in novel coherent and incoherent radiation production techniques and electron diffraction [6], they are now operated near their field limits. On the other hand, significant research in X-band RF power and structures has pushed the field limits to nearly double those in S-band. Thus one is inspired to search for ways to deploy X-band RF photoinjectors.

In considering how to create new RF photoinjector designs in an as yet unexplored wavelength regime, it is convenient to employ a series of scaling laws [7] developed expressly for this purpose. If one has found a high-performing design, including optimized emittance compensation (management of transverse beam plasma oscillations [8]) at a given RF wavelength λ, one can create an entire "family" of similar designs from it. For example, one can take that design easily to another RF frequency by first preserving the acceleration dynamics through scaling the RF electric field amplitude as $E \propto \lambda^{-1}$, which obviously keeps invariant the total energy of the beam. Indeed Kim's dimensionless analysis [2] of photoinjector dynamics originally introduced the scaling parameter $\alpha_{RF}=eE_0\lambda/\pi m_e c^2$ (E_0 being the maximum

* Corresponding author. Tel.: +1 310 2064541; fax: +1 310 2064551.
E-mail address: rosen@physics.ucla.edu (J.B. Rosenzweig).

0168-9002/$ - see front matter © 2011 Elsevier B.V. All rights reserved.
doi:10.1016/j.nima.2011.05.046

cathode field), explicitly illustrating this scaling rule, which may be restated as requiring α_{RF}=constant within a design family.

Given this rule, the transverse beam dynamics are preserved by scaling the magnetic field as $B \propto \lambda^{-1}$. Collective beam properties (energy spread, beam aspect ratio) are also left unchanged by scaling the beam sizes and charge as $Q \propto \lambda$, $\sigma \propto \lambda$; with these rules the beam plasma frequency scales correctly as $k_p \propto \lambda^{-1}$. The beam emittance in this case scales as $\varepsilon \propto \lambda$. If at a given λ one simply wishes to operate at another charge, this requires only preserving the beam plasma frequency, *i.e.* its density, yielding the scaling of the rms beam sizes as $\sigma \propto Q^{1/3}$. In this case emittance compensation is preserved, with a final ε depending on the charge in a power law between $Q^{1/3}$ at low Q (thermal limit), to $Q^{4/3}$ at high charge (RF/chromatic aberration limit).

Both charge and wavelength scaling present practical limitations. In Q-scaling, at high charge the effects of image charge at the cathode cause strong deviations from optimized dynamics, for example. In this paper, however, we are more concerned with wavelength scaling. The present generation (family) of high field, 1.6 cell photoinjectors in S-band, with associated downstream focusing solenoid, employs a design $\alpha_{RF} \cong 1.6-2$. This type of design may not be scaled directly into X-band due to unreasonably high electric field amplitudes, exceeding 400 MV/m. This value is precluded by RF breakdown considerations.

The first high performance photoinjector design family in which emittance compensation was discovered originally in L-band [1]. It was a relatively long (12 cells) π-mode standing wave structure, or so-called integrated photoinjector, as electron beam creation and post-acceleration are integrated into a single device. With its length, relatively high energy (>10 MeV) could be reached without the beam leaving the structure, and suffering both transverse and longitudinal defocusing effects. With distributed acceleration quite low peak fields ($\sim$20 MV/m, $\alpha_{RF}<1$) can be used in L-band; levels could be scaled even to X-band. Unfortunately these integrated designs are standing wave, in which case the initial RF fill provokes a transient reflected wave. The klystron and its output window must be protected from this reflected wave, typically by use of an RF circulator. Unfortunately, at the needed RF power, such devices do not exist in X-band.

Thus an alternative design family is needed; one that in fact has not been brought into realization until now—the hybrid photoinjector. The hybrid device is an integrated structure consisting of low gradient initial standing wave (SW) gun cells (2 or 3) connected at the input coupler to even lower field, long traveling wave (TW) section. A schematic view of the hybrid photoinjector is shown in Fig. 1. This new and novel design strongly mitigates the RF reflection problem, as the SW section represents a small fraction ($\sim$10%) of the power usage, and the TW section is approximately impedance matched to the input waveguide. The RF coupling shown in Fig. 1 is accomplished in the third cell encountered by the beam, with the SW section electrically coupled to it on-axis. This mode of coupling is particularly fortuitous, as it is accompanied by a 90° phase shift in the accelerating field, resulting in strong velocity bunching effects on the beam that reverse the usual bunch lengthening induced after the gun exit in standard 1.6 cell photoinjectors. The electromagnetics of the 90° phase shift, as well as other relevant details of the RF design of the X-band version of the hybrid photoinjector are included in a companion paper in these proceedings [9].

2. Beam dynamics in the hybrid photoinjector: S-band background

The present initiative to develop an X-band hybrid photoinjector by the INFN-LNF/UCLA/La Sapienza collaboration follows an S-band hybrid that is now being constructed. High power testing and beam production measurements will follow in 2011 at UCLA. This first generation S-band hybrid has 1.5 cell SW and 9 cell TW sections, with most of the RF power passing through the device and being directed either to a load or to a 3 m SLAC-type linear accelerator located after a short non-accelerating gap in which one may inject the photocathode drive laser. A schematic drawing of the S-band hybrid low energy section is shown in Fig. 1. The 1.5 cells of SW section containing the photocathode gun is followed by a coupling cell with dual waveguide external feeds, needed for symmetrizing the RF fields and avoiding the emittance growth associated with RF dipole errors [10]. Downstream of the coupling cell one finds the TW section, which first yields velocity bunching and then subsequently acceleration. As is common in low gradient, integrated photoinjector, focusing solenoids are placed over the initial cells to control the beam, as transverse space-charge effects are more pronounced with low-α_{RF} designs [11,12]. Despite the need for focusing close to the cathode, the required solenoid fields are not high, peaking at $\sim$1.5 kG.

The hardware implementation of this scheme in the first S-band hybrid photoinjector (low energy section only) is shown in the RF engineering drawing given in Fig. 2. The performance of the beam in this case has been studied in detail in previous analyses. Simulations concerning the performance of the low

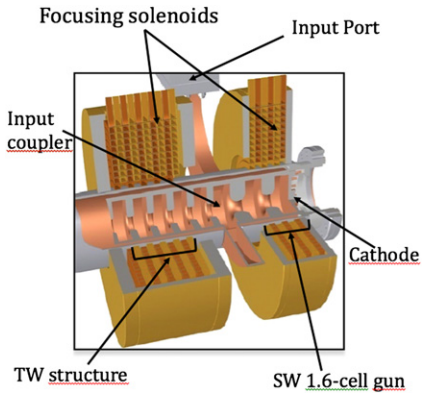

Fig. 1. Conceptual schematic of the low energy section of the hybrid photoinjector, showing standing wave photocathode gun section, external coupling cell with dual waveguide symmetrization, traveling wave section for velocity bunching and acceleration and focusing solenoids.

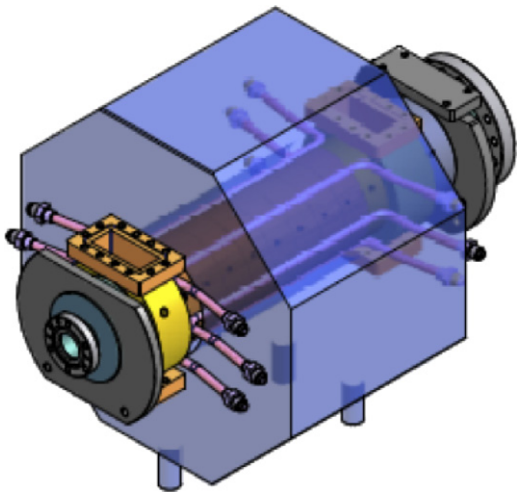

Fig. 2. Engineering view of INFN-UCLA-URLS S-band 2856 MHz hybrid photoinjector RF structure, with outline of downstream solenoid yolk indicated by shaded volume.

energy section alone concentrated on the possibility of using a low-charge, velocity bunched beam to extend the time resolution of ultra-relativistic electron diffraction (UED) [13]. They have also indicated that a beam of 1 nC can be strongly compressed, to less than 100 μm rms pulse length [14], while boosting the energy to 22 MeV with post-acceleration linacs. The higher energy beam may be used to efficiently produce incoherent (through inverse Compton scattering) and coherent THz radiation [15], e.g. from a super-radiant FEL.

In the present case, however, we are more interested in applications enabled by the first part of the hybrid that produces a low energy, highly compressed beam in X-band. These applications – particularly high frequency coherent radiation production and electron diffraction – depend strongly on achieving much higher brightness at low charge. Before proceeding to the discussion of possible applications in X-band, we review some recent results from S-band studies by the present collaboration that exploit the natural advantage of longer RF wavelength devices to produce higher charge beams. These results also anticipate the extension of the S-band device presently under construction to a version that (a) scales naturally to X-band, and (b) may be used at very high duty factor.

While scaling the design from S-band to X-band is straightforward in theory, practical limits require changes in both the RF and magnetostatic design approaches. As the field is limited by RF breakdown to 200 MV/m peak field, the SW section must be expanded to 2.5 cells to reach 3.5 MeV beam energy. This implies operation at 50 MV/m peak in S-band (2856 MHz), which means that the power needed to feed the SW part in S-band is only 2.1 MW. The TW part is fed through the coupler designed excite the structure to 14 MV/m average acceleration field, implying a downstream power flow of 18 MW for the shunt impedance of the TW section, and a total power $\sim$20 MW is obtained. A very small portion of the total input power is absorbed in the 9 cell TW section; this scheme is efficient only when the output power is directed to a long (typically 3 m) linac. If one would desire to optimize the structure to use lower input power more efficiently, the shunt impedance of the TW section should be raised considerably, and the coupling cell redesigned accordingly.

The focusing scheme is provided by solenoid magnets placed upstream (with a symmetrizing bucking coil to cancel the longitudinal field at the cathode) and downstream of the coupling waveguide. These two coils are located within separate yoke assemblies, with the downstream yoke located between the input and output waveguide, as indicated in Fig. 2. The peak solenoid field, as in the 1.5 SW cell design, does not exceed 1.5 kG. A further solenoid is needed downstream of the hybrid structure to control the beam size during velocity bunching, and the concomitant dramatic increase of transverse space-charge forces. The details of the similar magnetic field profile obtained from the solenoid array are discussed below in the scaled X-band case.

As stated above, the S-band design is more suited for high charge production, which we take advantage of, to enable a compact, novel plasma wakefield acceleration (PWFA) scheme, discussed below. The beam dynamics in the hybrid with solenoid focusing were simulated using a laser injected with uniform radial distribution having a hard-edge cut-off at $r=3$ mm, while employing a longitudinal pulse shape of 2.2 ps rms. The results of optimization using the simulations are summarized in Figs. 3 and 4.

In Fig. 3(a), the evolution of the mean energy as a function of z is shown. Inside the hybrid structure, the beam is first injected and accelerated in the SW region. After the coupling cell the beam finds itself near the zero-crossing of the RF wave in the TW section, and the beam initially suffers slight deceleration. As the 3.5 MeV beam slips in phase due to its deviation from the speed-of-light phase velocity, it eventually begins to accelerate.

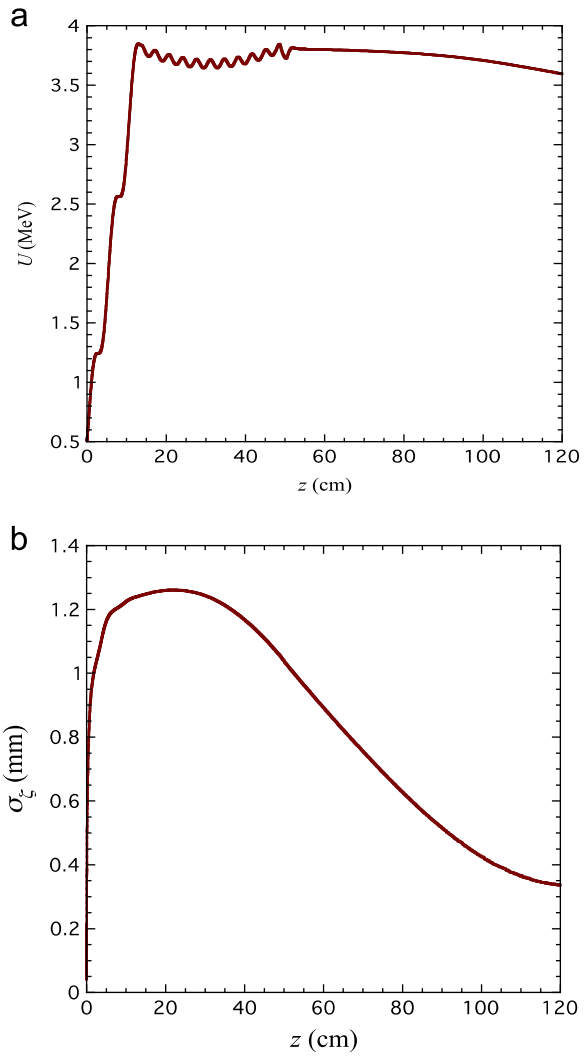

Fig. 3. Evolution of mean beam energy (a) and rms bunch length σ_ζ (b) in the S-band hybrid; beam charge 2 nC.

In Fig. 3(b), we give the evolution of the rms bunch length σ_ζ. The beam undergoes notable compression, by a factor of 3.5, producing a $\sim$1 ps rms pulse, with nearly 1 kA peak current, about 75 cm downstream of the structure exit.

We note that the phase between the final SW cell and the coupling cell (which serves as entrance to the TW section) is nominally $\pi/2$. One may change this phase, which controls the subsequent compression and acceleration of the beam, by detuning the temperature and thus the resonant frequency of the SW section. This phase tuning range is limited by the need to efficiently add power into the section, but is comfortably $\pm 15^\circ$. One may also make overall phase adjustments with the timing of photocathode drive laser injection. This subject is discussed further in a companion manuscript that concentrates on the RF behavior of the structure [9].

As the best emittance compensation performance occurs roughly at the transverse (space-charge dominated) waist, we optimized the dynamics to place the transverse and longitudinal waist at the same position in z. This gives "6D emittance compensation", with the shortest beams occurring simultaneously with low transverse emittance ε_n. The beam size evolution is shown in Fig. 4(a), with that of ε_n given in Fig. 4(b). The minimum emittance of this very high current beam after

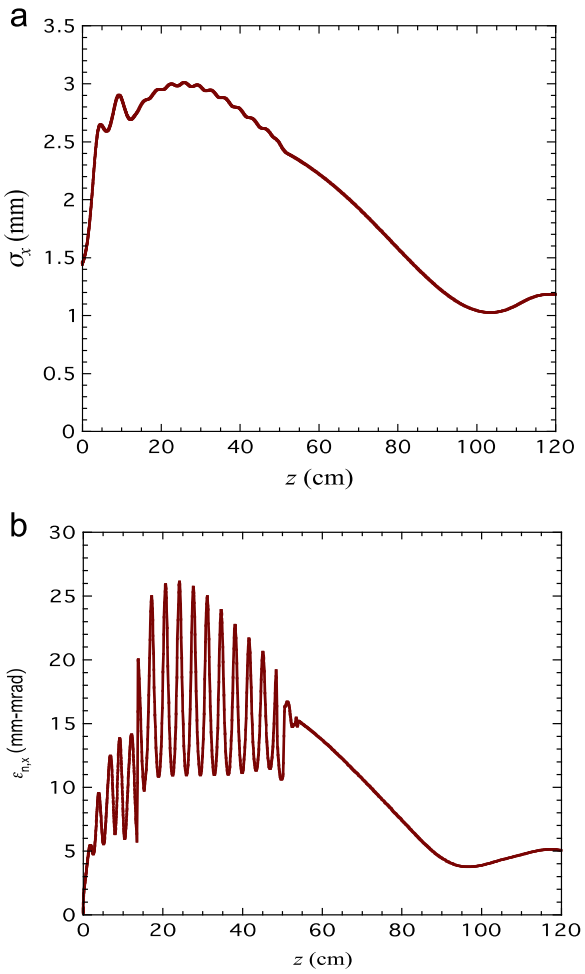

Fig. 4. Evolution of transverse beam size σ_x (a) and normalized emittance ε_n (b) in the S-band hybrid; beam charge 2 nC.

compensation, including 1.1 mm-mrad of thermal emittance is $\varepsilon_n \cong$ mm mrad, which is small enough to enable the PWFA application we explore in the next section.

3. Production of exponential energy spectrum electron beams by a hybrid-driven PWFA

We now discuss the application of the 2 nC beam from the S-band hybrid with the beam characteristics given above to a novel problem, that of mimicking the space radiation environment. This is a critical application, as damage of space-craft electronics in radiation belts presents many challenges in mission survivability. Space radiation has diverse sources and may consist of electrons, protons, ions and photons. In accelerating the charged particles, unlike in standard man-made accelerators such as linacs that function well only in producing nearly monochromatic particle beams, acceleration in nature is often stochastic due to the existence of many competing resonant waves. This scenario as a rule leads to energy spectra characterized by an exponential or power-law distribution. For instance, in the Earth's radiation belts, there is an exponential distribution of electrons up to ~10 MeV (known as "killer electrons", which provokes highly complex patterns of radiation damage) [16], with an e-folding in the MeV range. Ground-based conventional accelerators cannot reproduce the exponential electron beam spectrum occurring in space, and a typical approach to ground-based radiation hardening testing involves investigating the impact of radiation at multiple monochromatic energies, and then extrapolating the results to other energies based on models and assumptions. These methods are limited in energy range, laborious and expensive, and inherently do not capture the physics of specific scenarios.

Recognizing the need for such exponential spectra, Hidding et al. have recently proposed that a laser wakefield accelerator LWFA [17] be used to mimic space radiation environments. This approach is based on capture of electrons from the background plasma by waves excited with fs-duration, terawatt peak power lasers. While the single-shot spectra obtained from this approach limits the average flux, and thus the applicability of these new sources of the relativistic electrons for ground-testing of space-craft electronics. On the other hand, accelerators may produce extremely high average power; with a 1 kHz overall repetition rate, and moderate beam loading of the RF structure (100 beam pulses per 4 μs RF fill), one may obtain 200 μA of average current from S-band hybrid discussed above, giving a beam power equivalent to that of typical clinical linac.

To convert the energy distribution of this initially quasi-monochromatic stream of electrons, we thus propose to use the PWFA in the blowout regime [18], where the beam density exceeds that of the ambient plasma electrons, $n_b > n_0$. With an rms bunch length σ_ζ of 600 μm (2 ps), and the condition for most

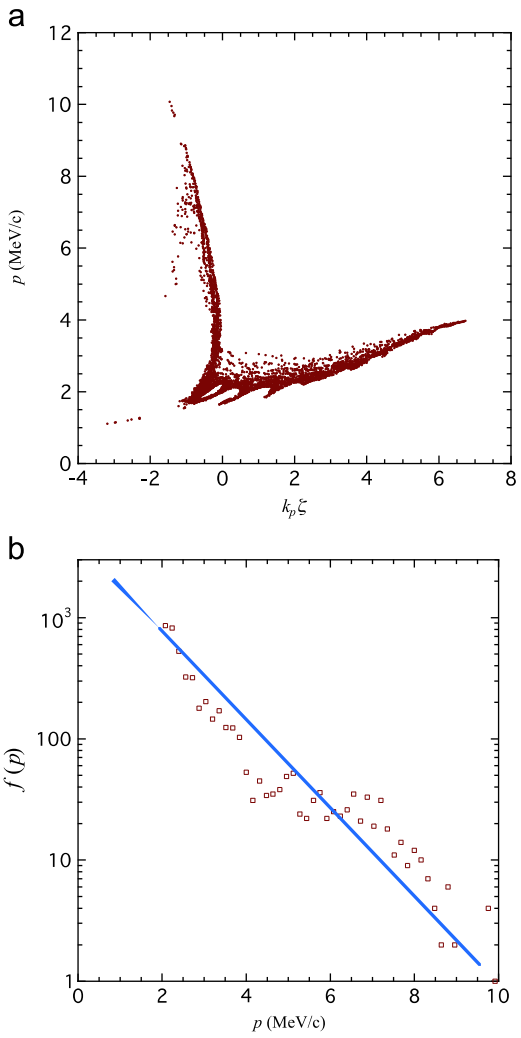

Fig. 5. (a) Longitudinal phase space after 4 cm of plasma; with (b) associated relativistic momentum distribution function $f(p)$, with exponential fit shown for comparison.

efficient wakefield deceleration on the beam $k_p\sigma_\zeta \cong 2$, where the plasma wave-number $k_p = \sqrt{4\pi r_e n_0}$, we deduce that $n_0 \cong 3 \times 10^{14}\,\mathrm{cm}^{-3}$. This parameter was in fact our goal in the present study; as it is within the reach of a hollow cathode arc source UCLA has been developed previously for PWFA applications [19].

This scenario was simulated using the 2D particle-in-cell (PIC) code OOPIC Pro [20]. In order to achieve the blowout regime, where the beam propagates with the transverse beam size σ_x stabilized through ion focusing, the beam should be smaller than $\sigma_x \approx 200\,\mu\mathrm{m}$. This condition can be satisfied by use of strong solenoidal focusing, starting from the beam shown in Fig. 3.

The beam longitudinal head is not strongly affected by the causal longitudinal plasma wakefields, while the core, with largest linear density, is strongly decelerated. The tail of the beam, $\zeta < -2\sigma_\zeta$, with much smaller linear density, is accelerated at up to twice the maximum rate of deceleration in the core. By decelerating the core until it begins to become non-relativistic (Fig. 5(a)), one obtains an approximately exponential momentum (nearly equivalent to the energy in the relativistic regime) spectrum from 2 to 10 MeV/c.

4. Beam dynamics in the hybrid photoinjector: extension to X-band

Much of the basis for scaling the hybrid photoinjector to X-band operation has already been discussed above. The field limitation of 200 MV/m peak on-axis has obviously been taken as a boundary condition in choosing the S-band RF structure from which we scale. The focusing solenoid may not be scaled directly, however, as the fields and concomitant current densities become more challenging, yet achievable with some modifications. Noting the peak magnetic fields needed are similar to those used for an X-band SW photoinjector [21] operated at SLAC (~6 kG, as expected from scaling), we modified this design of the solenoid around the RF structure itself to arrive at one suitable for emittance compensation in the hybrid case. The magnetic field used for LANL PARMELA simulations [22] is shown in Fig. 6; note the change in length and field scales by 4, as expected.

As we are more interested in the brightness frontier and applications enabled by ultra-short, low emittance beams, we also perform charge scaling, examining for our example here a quite small charge case, Q=6.75 pC, launched with rms pulse

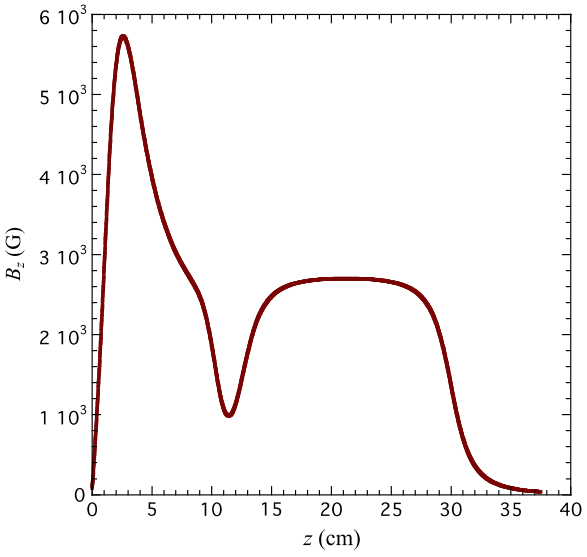

Fig. 6. Solenoid magnetic field profile for beam dynamics simulations of X-band hybrid photoinjector.

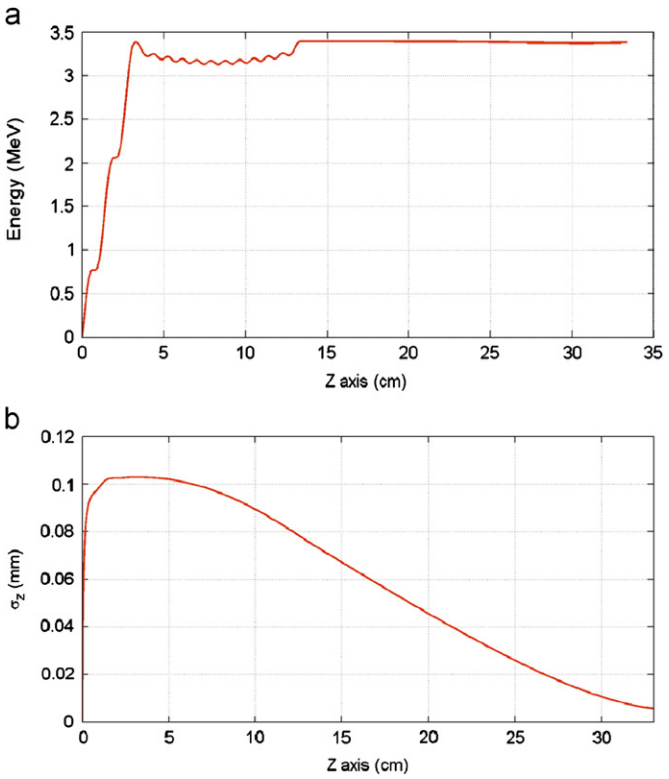

Fig. 7. Evolution of mean beam energy (a) and rms bunch length σ_ζ (b) in the X-band hybrid; beam charge 6.75 pC.

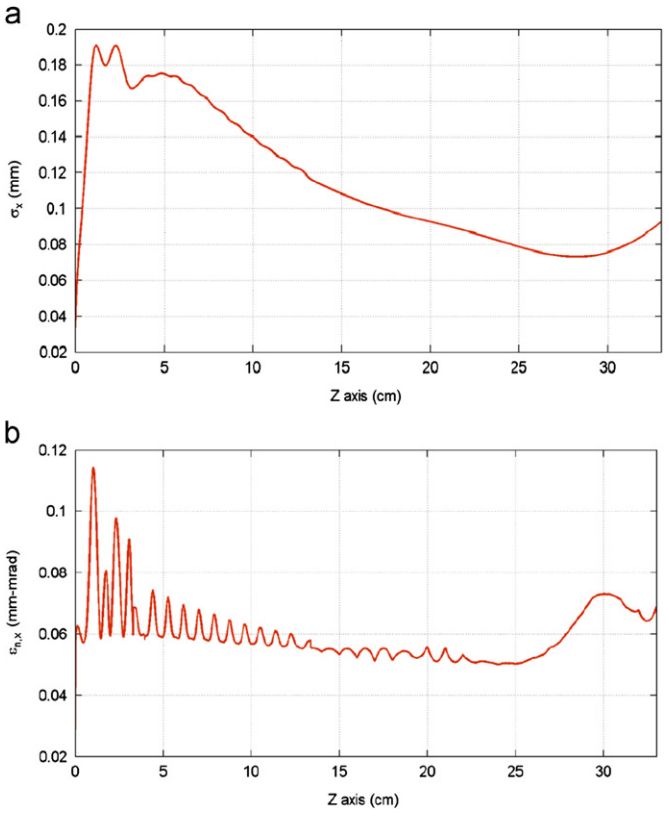

Fig. 8. Evolution of transverse beam size σ_x (a) and normalized emittance ε_n (b) in the in the X-band hybrid; beam charge 6.75 pC.

length 125 fs, having a hard-edge radial distribution cut-off at $r=190$ μm. The performance obtained in this case is summarized in Figs. 7 and 8, and it is impressive. The rms bunch length descends to $\sigma_\zeta \approx 5$ μm (16 fs), with an associated peak current of ~165 A. The emittance is extremely good with little need for compensation at this charge level; it is kept near $\varepsilon_n = 6 \times 10^{-8}$ mrad. With this combination of extreme short pulse and low emittance, the brightness of this beam is remarkable: it is $B_e = 2I/\varepsilon_n^2 = 9 \times 10^{16} A/(\text{mrad})^2$, which is over *two orders of magnitude higher* than the LCLS photoinjector beam after compensation. We next examine two applications directly enabled by this state-of-the-art beam: generation of multi-THz coherent Cherenkov radiation, and ultra-fast electron diffraction.

5. Application: coherent Cherenkov radiation from dielectric tubes

The use of dielectric wake tubes in the THz regime has many compelling applications, the promise of which has led to considerable recent work in UCLA-centered collaborations. Most compelling among them is GV/m-class acceleration [23] for future high energy physics colliders, and generation of high power, narrow-band THz radiation [24]. The key element in these schemes is to achieve short pulse electron beams, as the wake amplitudes produce scale roughly as $E_z \propto Q/\sigma_\zeta^2$, in modes of frequency up to $\omega_z \sim c/\sigma_\zeta$.

The field scaling given above is valid only when the aperture of the dielectric tube employed (see, e.g., Fig. 9) a is equivalent or smaller than σ_ζ. Both of our recently published experiments were performed at significantly higher energy, where the geometric emittance is smaller by the factor $\beta\gamma$, and the space-charge forces

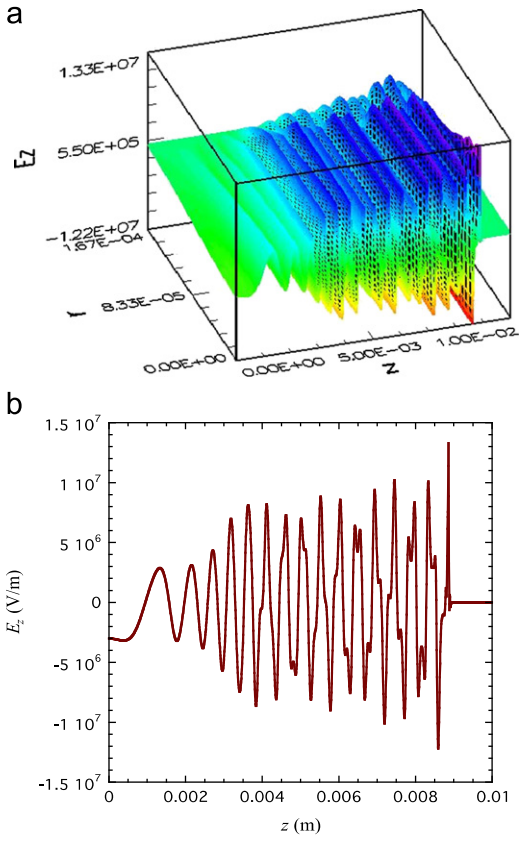

Fig. 9. (a) Simulation (OOPIC) of longitudinal wakefield with 6.75 nC, $\sigma_\zeta = 5$ μm, in SiO_2 tube of inner radius $a=100$ μm, outer radius $b=167$ μm; (b) on-axis line-out of field E_z.

are negligible. Thus even with a small normalized emittance, the focusability of the beam produced at 3.5 MeV by the X-band hybrid does not permit use of appropriately small a. The result of this is the excitation of a wake diminished in amplitude by $\sim a/\sigma_\zeta$, but having many harmonics excited by the impressively short pulse.

In fact, the beam produced in simulation permits apertures used with longer beams in previous experiments, and we employ one of the tubes used in the SLAC FFTB experiments where multi-GV/m breakdown thresholds were discovered (Ref. where 1-cm-long quartz dielectric tubes of inner radius $a=100$ μm, and outer radius $b=167$ μm). The results of OOPIC simulation of this case are shown in Fig. 9. Longitudinal wakes of 13 MV/m are produced, with an associated electromagnetic power of ~1 MW produced. This coherent radiation contains many harmonics, up to 5 THz, as can be seen from the wave train shown in Fig. 9(b). Note that the higher harmonics are more pronounced in the lead portion of the wave train, as they have higher group velocity in the structure. We have recently observed this effect in multi-pulse wake excitation experiments at the BNL ATF [25].

There are two novel aspects of this scenario. The first is that the multi-mode wave train contains a number of components at unprecedented high frequency, as the bunch length is shortened by an order of magnitude over previous sources. As the Cherenkov emission favors high frequency, the power at these frequencies is not negligible, despite the small beam charge. A multi-mode wave train provides new opportunities in tuning the radiation source, beyond changing out tube geometries [24]. One may provide resonant filters to pass only one component of the radiation at a time, and also use width of the filter to control the bandwidth further. This approach promises to expand the range of applications [26] enabled by this new class of high power, narrow-band THz source.

6. Application: ultra-fast electron diffraction

The application of a highly compressed beam to ultra-fast electron diffraction (UED) has been examined in the context of the S-band hybrid previously [13]. While the UCLA program has shown excellent progress in UED, including the first demonstration of a time-resolved UED-based measurement [27], in order to obtain the 10^7–10^8 electrons needed for a useful diffraction pattern, the beam is limited by longitudinal space-charge effects to 100 fs pulse lengths [28]. As noted above, the simulated beam output from the hybrid has roughly the same charge, permitting a robust measurement with an order of magnitude faster time resolution.

The low emittance of the X-band hybrid beam is also critical to the UED application. In order to resolve adjacent maxima in the diffraction pattern, the spacing of these maxima must be approximately twice that of the beam rms angular spread. As both of these angles scale with the momentum $\beta\gamma m_e c$, the resolving power ratio is momentum independent, and may be stated as

$$R = \frac{\lambda_C \sigma_x}{2\varepsilon_n d}$$

where λ_C is the Compton wavelength, d is the spacing of atoms (typically ~2 Å) in the matter under study and σ_x is the beam size at the sample that gives rise to the scattering. Using the parameters at the 6D compensation point from Fig. 8, we have a resolving power $R=8$. Better resolution of the diffraction pattern is obtained from a larger beam, but this case is in fact interesting, as an 80 μm spot size is consistent with easily obtainable high-intensity laser spots in laser-excited experimental scenarios.

The advantages of using the X-band hybrid for UED are based on high fields, which give low emittances, and on velocity bunching, which gives impressively short pulses. There are drawbacks, however, in this approach, particularly in the background from the dark current that will be greatly enhanced by 200 MV/m cathode fields. This can be mitigated by use of collimations, but will be qualitatively different from the present generation UED systems.

In our desire to present a unified simulation set for both the coherent Cherenkov radiation and UED applications, we have utilized thus far a charge that exceeds what one minimally needs for single-shot diffraction, by at least one order of magnitude. If we scale Q down to 0.25 pC (1.5×10^6 electrons), then the achieved minimum pulse length of $\sigma_\zeta=0.6$ μm (2 fs) is truly impressively short. Meanwhile the normalized emittance is also reduced to $\varepsilon_n=2-10^{-8}$ mrad. The scaling results in an integrated flux of electrons only a factor of 3 smaller at the 6D compensation point, with the same angular spread, but a pulse nearly an order of magnitude faster. This case will be studied more in the future.

7. Conclusions

The X-band hybrid SW/TW photoinjector represents an obvious extension and evolution of this new class of powerful device. Scaling from S-band seems possible, with some consideration to the maximum fields, both electromagnetic and magnetostatic that are experimentally permitted. The details of the structure design and performance of the X-band hybrid system are provided in a companion paper [29]. The brightness of the beam produced, particularly at low charge, enters into a new regime, permitting a wide variety of promising new applications, in radiation production, electron diffraction and use of wakefield acceleration. In this regard, it should be noted that the PWFA example given as an illustration of S-band capabilities could be also implemented, via familiar scaling rules, in X-band as well.

The authors acknowledge useful discussions with S. Tantawi, G. D'Auria and A. Murokh. This work was supported by the U.S. Department of Energy under Contracts nos. DE-FG02-07ER46272 and DE-FG03-92ER40693, and the Office of Naval Research under Contract no. ONR N00014-06-1-0925.

References

[1] B.E. Carlsten, Nucl. Instr. and Meth. A 285 (1989) 313.
[2] K.J. Kim, Nucl. Instr. and Meth. A 275 (1989) 201.
[3] J. Rosenzweig, et al., Nucl. Instr. and Meth. A 341 (1994) 379.
[4] P. Musumeci, et al., Phys. Rev. Lett. 100 (2008) 244801.
[5] R. Akre, et al., Phys. Rev. ST Accel. Beams 11 (2008) 030703.
[6] P. Musumeci, et al., Rev. Sci. Instr. 81 (1) (2010) 013306.
[7] J.B. Rosenzweig, E. Colby, Adv. Accel. Concepts (1995) 724 (AIP Conf. Proc. 335).
[8] L. Serafini, J.B. Rosenzweig, Phys. Rev. E 55 (1997) 7565.
[9] A. Valloni et al., Nucl. Instr. and Meth., these proceedings.
[10] J.B. Rosenzweig, S. Anderson, X. Ding, D. Yu, in: Proceedings of the Particle Accelerator Conference, 1999, 2042.
[11] E. Colby, UCLA Ph.D. Thesis, FERMILAB-THESIS-1997-03, (FNAL, 1997).
[12] Ph. Piot et al., Conceptual Design of the XFEL Photoinjector, TESLA FEL Report, 2001–2003.
[13] P. Musumeci, et al., Microsc. Microanal. 15 (2009) 290.
[14] J.B. Rosenzweig et al., AIP Conference Proceedings 877, 2006, 635–641.
[15] A. Fukasawa et al., in: Proceedings of the International Particle Accelerator Conference, Kyoto, Japan UPEC021 (JACoW, 2010), p. 1758.
[16] R.B. Horne, Nat. Phys. 3 (9) (2007) 590.
[17] B. Hidding, et al., Nucl. Instr. and Meth. 636 (2011) 31.
[18] J.B. Rosenzweig, B. Breizman, T. Katsouleas, J.J. Su, Phys. Rev. A 44 (1991) R6189.
[19] N. Barov, J.-P. Carneiro, H. Edwards, W. Hartung, M.J. Fitch, K. Bishofberger, J.B. Rosenzweig, in Proceedings of the Particle Accelerator Conference (IEEE, 2001), 126.
[20] D.L. Bruhwiler, et al., Phys. Plasmas 10 (2003) 2022.
[21] A. Vlieks et al., in Proceedings of the High Energy Density and High Power RF: fifth Workshop AIP CP625, 2002, 107.
[22] L. Young J. Billen, Tech. Rep. LA-UR-96-1835, LANL, 1996.
[23] M.C. Thompson, et al., Phys. Rev. Lett. 100 (2008) 21.
[24] A.M. Cook, et al., Phys. Rev. Lett. 103 (2009) 095003.
[25] G. Andonian, O. Williams, X. Wei, P. Niknejadi, E. Hemsing, J.B. Rosenzweig, P. Muggli, M. Babzien, M. Fedurin, K. Kusche, R. Malone, V. Yakimenko, Appl. Phys. Lett. 98 (2011) 202–901.
[26] G.L. Carr, et al., Nature 420 (2002) 153.
[27] P. Musumeci, et al., Appl. Phys. Lett. (2010) 063502.
[28] P. Musumeci, J.T. Moody, R.J. England, J.B. Rosenzweig, T. Tran, Phys. Rev. Lett. 100 (2008) 244801.
[29] B. Spataro, et al., Nucl. Instr. and Meth. A (2011). doi:10.1016/j.nima.2011.04.057.